Integration of Plasmonic Au Nanoparticles in TiO_2 Hierarchical Structures in a Single-Step Pulsed Laser Co-Deposition

Beatrice Roberta Bricchi[a], Matteo Ghidelli[a], Luca Mascaretti[a], Andrea Zapelli[a], Valeria Russo[a,b], Carlo Spartaco Casari[a,b], Giancarlo Terraneo[b,c], Ivano Alessandri[d,e], Caterina Ducati[f], Andrea Li Bassi[a,b]

[a] *Micro- and Nanostructured Materials Laboratory, Department of Energy, Politecnico di Milano, via Ponzio 34/3, 20133, Milano, Italy.*

[b] *Center for Nanoscience and Technology – IIT@Polimi, via Giovanni Pascoli 70/3, 20133, Milano, Italy.*

[c] *Laboratory of Supramolecular and Bio-Nanomaterials, Department of Chemistry, Materials, and Chemical Engineering "Giulio Natta", Politecnico di Milano, Via L. Mancinelli 7, 20133, Milano, Italy.*

[d] *Department of Information Engineering, Chemistry for Technologies Laboratory, University of Brescia and INSTM UdR Brescia, Via Branze 38, 25123 Brescia, Italy.*

[e] *INO-CNR Brescia Unit, via Branze 45, 25123, Brescia, Italy.*

[f] *Department of Materials Science & Metallurgy, University of Cambridge, 27 Charles Babbage Road, CB3 0FS, Cambridge, UK.*

Abstract

The plasmonic resonance of noble metal nanoparticles (NPs) can be exploited to enhance the photoresponse of wide band gap oxides in view of several solar energy applications. Here, we demonstrate single-step synthesis of plasmonic Au nanoparticles integrated in TiO_2 hierarchical nanoporous layers through a vapor phase pulsed laser co-deposition approach. Specifically, we report the fabrication and characterization of Au NPs-decorated TiO_2 forest-like systems with tunable porosity and density as well as the morphological/structural evolution as a function of Au content and we discuss the corresponding optical properties. The effect of post-deposition thermal treatment has been investigated as well in order to control TiO_2 crystallization and Au NPs nucleation and growth. Optical analyses show the onset of characteristic plasmonic resonance of Au NPs with the increase of film absorption in the visible range. Preliminary tests of photodegradation of methyl orange dye indicates that the integration of Au NPs leads to a significant increase of the catalytic activity of nanoporous TiO_2. Our results suggest the potentiality of this approach for the synthesis and the integration of metallic NPs within wide band gap semiconductors, while paving the way toward novel plasmonic-based devices.

Keywords

Au nanoparticles; Nanostructured TiO_2 films; Plasmonics; Pulsed Laser Deposition; Photocatalytic application.

1. Introduction

In recent years, the need for increasingly higher performances in advanced technological applications has pushed the interest toward novel materials with advanced functionalities. Wide band gap semiconducting oxides are currently employed as photoanodes in the fields of photovoltaics [1,2], solar water splitting [3], and photocatalysis [4,5]. Titanium dioxide (TiO_2) is largely investigated for the mentioned applications due to its large chemical stability and availability, together with the lack of toxicity [6,7]. Nevertheless, the wide band gap (3.2 eV for the anatase phase [8]) and the high recombination rate of the photogenerated charge carriers constitute significant limitations to a successful employment of this material for photoconversion processes [7].

A strategy to improve the photoresponse is the integration of metal nanoparticles (NPs) in the oxide photoanodes, which is raising a great interest due to their plasmonic properties and their potential for enhancing the photoresponse of materials and devices for several applications [5].

The size confinement of metallic NPs at the nanometer scale enables the activation of the localized surface plasmon resonance (LSPR), i.e. collective oscillation of conduction electrons in response to an external electric field, triggered by selected wavelengths [3,9]. The LSPR frequency depends on the selected material, the dielectric constant of the surrounding environment, the NPs size and shape distribution as well as the distance and the interaction between them [10,11]. By tuning these parameters, it is possible to design plasmonic NPs that can absorb and scatter selected wavelengths [12] with a very large cross-section [9]. These fascinating properties can pave the way to a number of possible applications including catalysis [4,5], chemical sensors and biosensors [13,14], substrates for surface enhanced Raman scattering (SERS) [15,16], and solar energy [1,17].

Typically, gold and silver NPs are mostly employed for achieving plasmonic effects because of their plasmonic resonance peak in the visible and near IR range [3,18]. Among them, Au is mostly used because it is chemically inert, while limiting corrosion effects under photocatalytic conditions [9,19,20].

Recent studies on the integration of metal NPs in TiO_2 have reported an increment in light absorption in the visible range and a reduction of recombination rate of photogenerated charge carriers [1,4,21]. However, adding plasmonic metallic NPs could be interesting and beneficial also for other oxides employed in photoelectrocatalytic applications as well as ZnO [22] and Fe_2O_3 (hematite) [23,24] in order to increase their absorption and photoconversion capability.

Examples of integration of Au NPs in TiO_2 films using chemical or physical methods have been reported in the literature. For instance, Haruta *et al.* [25] embedded 20 nm-diameter Au NPs within TiO_2 demonstrating that the synthesis method strongly determines the final catalytic activity. For this purpose, they used chemical and physical methods as well as adsorption of preformed Au colloids, deposition-precipitation, co-sputtering and Chemical Vapor Deposition (CVD). More recently, a similar approach has been used by Valverde *et al.* [26] and Gomes Silva *et al.* [19] reporting the adsorption of colloidal Au NPs on TiO_2 surface for photovoltaic devices and for solar water splitting. Other possible chemical techniques are the photodeposition of Au on TiO_2 [20,27] and the chemical spray pyrolysis [28]. However, chemical approaches have some drawbacks including the use of aggressive solvents and the presence of remaining contaminants [29], while requiring a two steps procedure, namely the synthesis of Au NPs and subsequent infiltration in the TiO_2 films, which are typically nanoporous in order to achieve high surface area as required for the mentioned applications [30]. For these reasons, a proper dispersion of NPs within TiO_2 structures is difficultly achieved [1,26,31]. On the other hand, a physical method of synthesis allows the production of highly pure NPs without the presence of contaminants, keeping a good control of size distribution. Mubeen *et al.* [21] used the electron-beam evaporation method to obtain a film structure constituted of alternated Au and TiO_2 layers, then dewetting activated by post-thermal annealing enabled the formation of Au NPs. Another possible physical approach involves the use of reactive magneton sputtering, e.g. Rodrigues *et al.* [32] and Borges *et al*. [33,34] deposited TiO_2 films decorated with Au NPs exploiting a composite Ti/Au target managing to accurately tune the Au percentage and thus the film optical behavior. However, this technique is limited to

the production of compact films, while the fabrication of porous and nanostructured films with a large surface area is hindered.

Among other physical methods, Pulsed Laser Deposition (PLD) allows to tune several properties (i.e. composition/stoichiometry, morphology, structure) of the deposited films by carefully controlling the process parameters [35,36], therefore, it is a promising technique to integrate Au NPs in a semiconducting oxide as TiO_2. Indeed, PLD has been already exploited both for the production of (i) Au NPs with high purity and good control of size and morphology [37-40] and (ii) TiO_2 nanostructured films with a so-called hierarchical morphology for photocatalysis [41,42], photovoltaics [43-46] and photoelectrochemical water splitting [45-48]. In particular, the porosity and density of TiO_2 hierarchical films can be controlled by tuning the PLD process parameters, obtaining large surface area (from tens to hundreds m^2/g) [41,45,47] and a peculiar vertically-oriented morphology that can facilitate the transport of photogenerated charge carriers as well as produce an effective visible light scattering [30].

In this work, a PLD co-deposition approach for the synthesis of integrated Au NP-TiO_2 films has been successfully performed with a single-step procedure involving the ablation of a composite TiO_2-Au target. Specifically, we managed to finely disperse Au NPs through the whole thickness of TiO_2 film, while tuning its porosity as well as the Au percentage.

As main results, we show that: (i) Au NPs with size smaller than 10 nm can be homogeneously distributed throughout all the hierarchical structure of TiO_2 films; (ii) the post-deposition thermal treatment (500°C in air) allows Au NPs nucleation and/or growth while leading TiO_2 crystallization in anatase phase; (iii) the presence of Au NPs increases the absorption of the film the visible region and, in certain conditions, promotes the appearance of well-defined LSPR peak; (iv) preliminary tests of photodegradation of methyl orange show that the presence of Au NPs in TiO_2 nanoporous films significantly increases the catalytic action of the material.

2. Experimental details

PLD has been accomplished in a vacuum chamber equipped with mass flow controllers to tune the partial gas pressure. The laser pulses are focused on the target material through a viewport. The target is mounted on a roto-translational manipulator so that subsequent pulses hit the target in different position thus ensuring an uniform ablation. Co-deposited films of TiO_2 and Au have been synthetized by ablating a 2 inches TiO_2 target (99.9% pure, provider "Kurt J. Lesker") partially covered with Au plates (99.99% pure, provider "MaTeck") attached on the target surface. Au plates have been placed in order to have some subsequent laser shots on gold only, during the target motion. Ablation has been performed with a ns-pulsed laser (Nd:YAG, 2^{nd} harmonic, λ = 532 nm) with pulse duration 5-7 ns and repetition rate 10 Hz. The laser pulse energy was set at 170 mJ, corresponding to a laser fluence on the target of 3.5 J/cm^2. The employed substrates were Si (100) and soda-lime glass cleaned in ultrasonic bath with isopropanol and mounted on a rotating sample holder at a fixed target-to-substrate distance of 50 mm. Depositions were performed at room temperature with a pure O_2 background gas at two different pressures, 5 and 8 Pa, to study two different film morphologies, keeping a nominal film thickness of 1 μm. The Au content of the co-deposited films was controlled by varying the number of Au plates on target and the Au atomic percentage (% at.) in the deposited films was estimated by energy dispersive x-ray (EDX) spectroscopy with accelerating voltage of 15 kV. Table 1 lists the Au amounts studied at the two deposition pressures and the corresponding target area covered by Au. Notably, by varying the deposition pressure, the same Au target area corresponds to a different Au atomic percentage in the films because the deposition rate of species changes with background pressure and, therefore, the same thickness (1 μm) is achieved with different deposition times and so different shot numbers.

Au Target Area (%)	**5 Pa - Au % at.**	**8 Pa - Au % at.**
6.6	5	3.9
4.0	3.5	2.9
2.7	2.5	2.4
1.3	1.1	1.0
0.7	0.8	0.7
0.3	0.6	0.5

Table 1. *Atomic percentage of Au in the film measured by EDX and the corresponding target area.*

Post-deposition annealing treatments were performed in air in a Lenton muffle furnace with 4 °C/min heating ramp and 2 hours dwell at 500°C, the typical temperature for anatase crystallization [48]. A field emission scanning electron microscope (FEG-SEM, Zeiss Supra 40) was used to perform morphological characterization analyzing films deposited on Si (100) substrate.

TEM analysis was performed using a FEI Tecnai F20 FEG-TEM with acceleration voltage of 200 kV. The microscope is equipped with a Gatan OneView camera for image acquisition. Specimens of TiO_2+Au films were removed from the Si substrates and deposited on TEM Cu grids. The average diameter of Au NPs has been estimated by a statistical analysis on TEM images with the open source software ImageJ.

Structural characterization was carried out by X-Ray diffraction (XRD) and Raman Spectroscopy. XRD patterns were collected using a Bruker D8 Advance X-Ray diffractometer at 293 K (CuKα1 radiation - 1.5406 Å). The measurements were carried out in Bragg–Brentano geometry with a step–scan technique in 2θ range of 10–75°. Data were acquired by Lynx Eye detector in continuous scanning mode with a step size of 0.038° and time/step of 0.15 s. The crystallite size for the gold nanoparticles integrated in TiO_2 hierarchical films was determined by fitting the XRD data using Pawley method [49]. The Pawley method was carried out using the program-suite TOPAS from Bruker. Raman spectra were collected using a Renishaw InVia micro Raman spectrometer with an argon ion laser (514 nm), laser power at the sample of 1 mW and spectral resolution of about 3 cm^{-1}.

Optical transmittance and reflectance spectra were evaluated with a UV-vis-NIR PerkinElmer Lambda 1050 spectrophotometer with a 150 mm diameter integrating sphere in the range 250-2000 nm. All the acquired spectra were normalized with respect to glass substrate contribution.

The photocatalytic activity was evaluated by irradiating vessels containing 2.5 mL of a 10^{-5} M solution of methyl orange (MO) in the presence of Au-TiO_2 thin films deposited on Si substrates. The irradiation is provided by a solar simulator (Abet technologies, Sun 2000 Simulator, model 11016) at a working distance of 15 cm. Power was set equal to 550 W and irradiance to A.M. 1.5. Each support was masked to irradiate a

region with the same area (5x5 mm^2) and is kept at a temperature of 33°C, measured with a thermometer. A vessel containing the same aliquot of MO in the absence of any photocatalysts was taken as a reference. Before irradiating, each vessel was kept in dark for 1 hour, in order to take the contribution of adsorption into account. The photocatalytic activity was evaluated by monitoring the variation of the optical absorbance of MO. In particular, the absorbance of the MO band centered at λ=460 nm (ε=26800 M^{-1}) was utilized to calculate the concentration of dye solution as a function of irradiation time. The data obtained from different films were normalized to the film deposition time, and thus to the amount of TiO_2 deposited mass per unit surface.

3. Result and discussion

3.1 Morphology of as-deposited Au-TiO_2 films

Fig. 1a-d shows the SEM cross-section images of as-deposited pure TiO_2 and Au-TiO_2 films deposited at 5 and 8 Pa. The effect of O_2 background pressure on TiO_2 deposition has been already studied in previous works [41,43,47,50]: the higher the pressure, the higher the porosity and the lower the density (Fig. 1a, 1b). Specifically, in the deposition conditions explored (background pressure 5-8 Pa) the TiO_2 film density has been estimated in the range 1 - 2 g/cm^3, which means a corresponding film porosity from 50 to 70% [50]. The effect of Au addition in the film induces a slightly more compact structure as can be observed in Fig. 1c and 1d for both films deposited at 5 and 8 Pa. Indeed, by keeping a constant deposition time, the obtained thickness decreases with increasing Au content. Furthermore, Au plays a role on the morphological organization as well. Specifically, 5 Pa films (Fig. 1c) show a layered structure in which TiO_2 is separated by 10 nm-thick Au-rich layers which is originated by the target geometry (with alternated ablation of Au and TiO_2 target regions, see Experimental details), combined with the fact that in this deposition condition the pressure is not enough to induce significant Au NP nucleation and growth [40].

TEM analysis has been carried to unveil the nanoscale organization of Au NPs and TiO_2 films. Fig. 1e shows that the Au layer is not continuous, but is formed by very small Au NPs (less than 3 nm) very close to each other. On the other hand, in films deposited at 8 Pa, Au is in the form of NPs with an average diameter < 10 nm and homogeneously distributed in the porous nanostructures of TiO_2 (Fig. 1d), which indicates that the cluster-assembled growth promoted at 8 Pa leads to the formation of dispersed Au NPs (rather than organized in layers). From TEM analysis (Fig. 1f) also smaller NPs are visible and so the average diameter can be estimated around 5 nm.

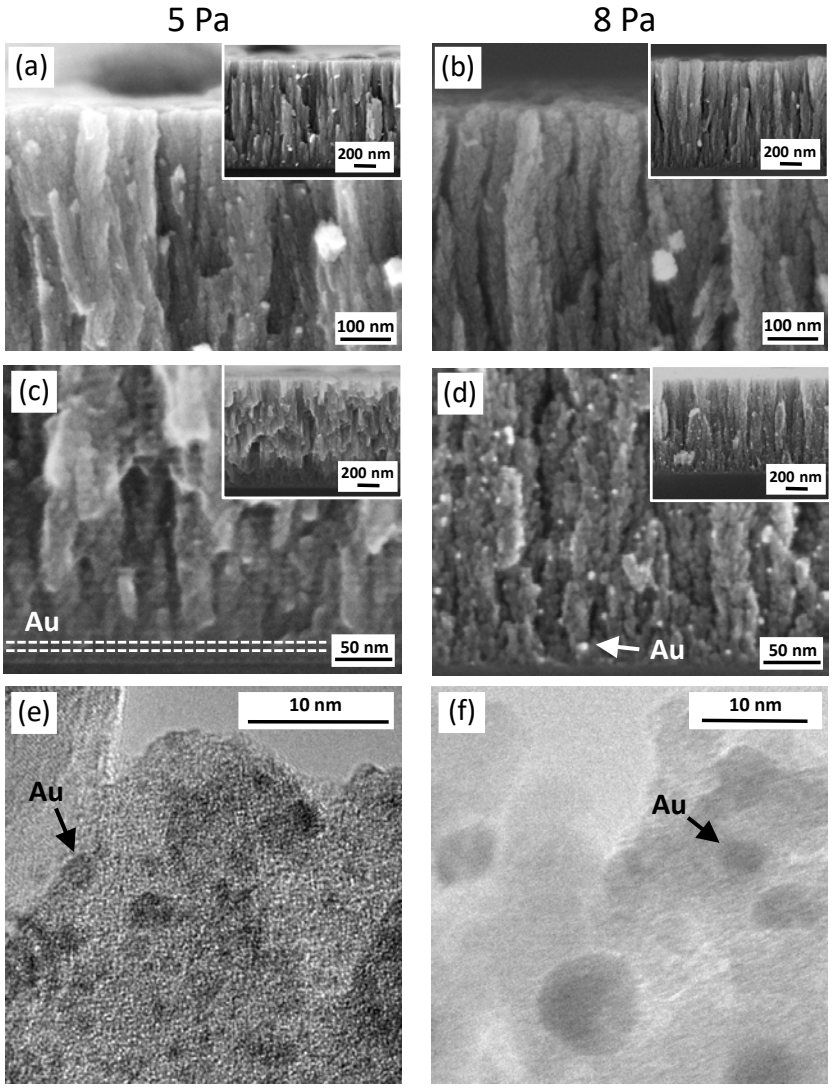

***Figure 1**. SEM (a-d) and TEM (e,f) images of Au-TiO_2 films deposited at 5 and 8 Pa with different Au contents. Pure 5 Pa TiO_2 film and with 3.5 % at. Au are reported in (a) and (c,e), respectively, while (b) and (d,f) report pure 8 Pa TiO_2 film and with 2.9 % at. Au, respectively.*

3.2 Effect of thermal treatment and Au content

Fig. 2 shows SEM and TEM images of selected samples after annealing treatment at 500°C for 2 hours (see Experimental details), which promotes the formation of TiO_2 nanocrystals with an average size of few tens nm partially merged with each other due to sintering effects [47,51]. The thermal treatment has an effect on Au structures, as well, providing the energy for the diffusion of Au atoms. The mechanisms governing the NPs formation and coarsening during a thermal treatment are Ostwald ripening and NPs diffusion and subsequent coalescence [52-54].

From the analysis of different TEM images it was possible to estimate the size of the observed Au NPs: the annealed Au-TiO_2 film deposited at 5 Pa with 3.5% at. Au (Fig. 2d) shows larger Au NPs than the corresponding as-deposited film (Fig. 1e), indeed the average diameter increases from less than 3 nm to around 5 nm after thermal treatment. Conversely, an apparent decrease in the average Au NP diameter, from ~5 nm down to 3 nm, is observed in the Au-TiO_2 film deposited at 8 Pa with 2.9% at. Au after thermal treatment. We can suppose that Au atoms or very small Au atomic clusters, probably already present before annealing but not visible by TEM, aggregate and grow upon thermal treatment thus becoming detectable.

Furthermore, the effect of Au content on NP size in annealed films was investigated by TEM. Au-TiO_2 films deposited at 5 Pa show a slight increase in Au NPs size vs. Au content; i.e. films with 0.8% at. (Fig. 2c) and 3.5% at. Au (Fig. 2d) exhibit NPs with average diameter of 3 and 5 nm, respectively. Instead, Au-TiO_2 films deposited at 8 Pa with Au content of 0.7% at. (Fig. 2g) and 2.9% at. (Fig. 2h) reveal Au NPs with almost constant average size, around 3 nm. As expected, at both deposition pressures, the Au NPs number density increases with the amount of Au (Figs. 2a-b, 2e-f).

From selected TEM images (see e.g. Fig.2h) it was possible to analyze the spacing of the characteristic lat-tice plane fringes of Au NPs and TiO_2 domains of the annealed films. The spacing for Au NPs is equal to 0.236 nm, compatible with Au [111] fcc structure, while, for the TiO_2 regions it confirms the presence of anatase phase.

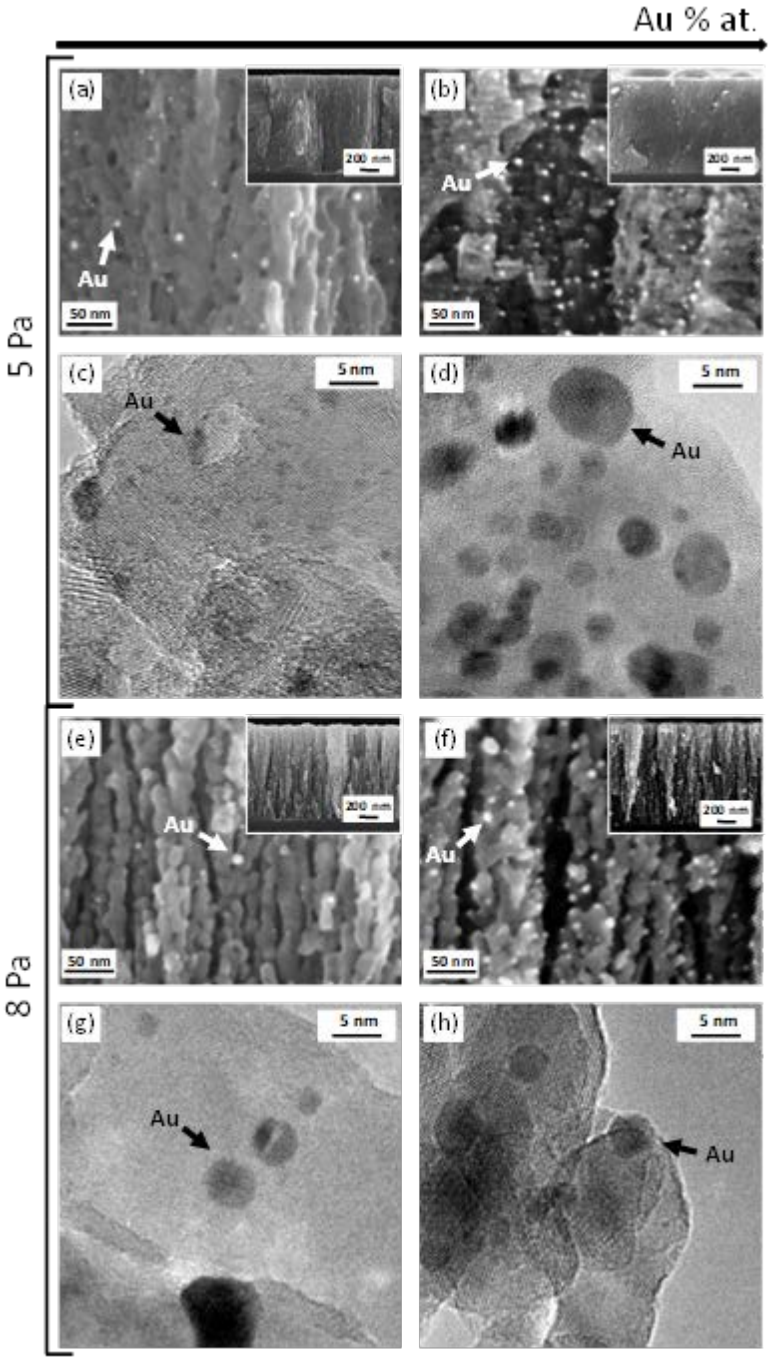

Figure 2. *SEM (a, b, e, f) and TEM (c, d, g, h) images of annealed Au-TiO_2 films deposited at 5 and 8 Pa with different Au contents. 5 Pa Au-TiO_2 films with 0.8 and 3.5 % at. Au are reported in (a, c) and (b, d), respectively; 8 Pa Au-TiO_2 films with 0.7 and 2.9 % at. Au are shown in (e, g) and (f, h), respectively.*

Further structural analysis of Au-TiO_2 films has been performed by means of XRD and Raman spectroscopy. Fig. 3a and 3b report the XRD analysis of film deposited at 5 and 8 Pa, respectively, with different amounts of Au, before (i.e. as deposited) and after the annealing treatment.

Au peaks are detectable only for the highest Au contents. Specifically, for films with 3.5 and 2.9% at. Au deposited at 5 and 8 Pa, respectively, the Au characteristic peaks located at 38.19 and 44.39° are visible [55] both before and after annealing, pointing out the presence of crystalline Au. Specifically, the Au [111] peak of as-deposited films has a very low intensity, corresponding to very small Au crystalline domains (smaller than 3 nm), while the anatase peaks are not detected, suggesting an amorphous TiO_2 structure, as expected [41,51].

For these films it has been possible to estimate the Au crystalline domain size after annealing, through Pawley fitting (see Experimental details), i.e. 8 and 12 nm at 5 and 8 Pa, respectively. The difference between Au size evaluated by XRD and TEM is not unexpected, indeed TEM allows a direct observation of selected NPs, while XRD provides the mean scattering domain size. Furthermore, these techniques are sensitive to different orders of magnitude of investigated material volume and, finally, XRD is sensitive to larger NPs whereas the smallest ones are simply not detected.

At both pressures, annealed films show the characteristic TiO_2 anatase peaks (Figs. 3a, 3b); no shift is detected despite the presence of Au, which rules out a possible doping effect [56]. On the other hand, a slight variation of the full width at half maximum (FWHM) is detectable, which means that the Au content affects the TiO_2 crystalline domain size. Figure 3c shows the average TiO_2 domain size evaluated through Scherrer's equation based on the analysis of TiO_2 [101] peak. Notably, the average size is strongly dependent on deposition pressure, being equal to about 40 and 25 nm for TiO_2 films deposited at 5 and 8 Pa, respectively, in agreement with a stronger sintering effect in more compact films [41]. Then, the average crystalline domain size decreases with the increase of Au content at both deposition pressures (Fig. 3c, from 45 to 35 nm for films deposited at 5 Pa with 3.5% at. Au; from 26 to 22 nm for films deposited at 8 Pa with 2.9% at. Au). The Raman analysis of the annealed Au-TiO_2 films confirms XRD results (see SI1). Indeed, the characteristic

anatase Raman peaks are detected, but a slight increase (2 cm^{-1}) in the Eg_1 peak full width at half maximum (FWHM) is observed when moving from pure nanoporous TiO_2 to Au-TiO_2 films with 3.5% at. Au (at 5 Pa) and 2.9% at. Au (at 8 Pa).

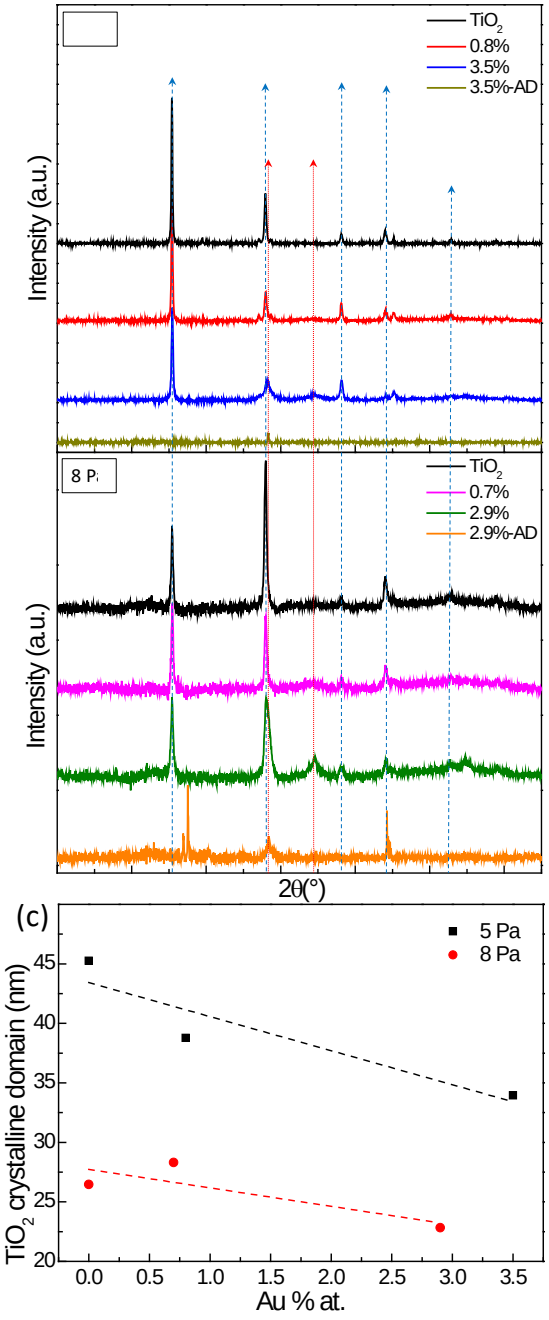

Figure 3. *XRD of Au-TiO_2 films deposited at (a) 5 Pa and (b) 8 Pa with different amount of Au as deposited (AD) and after annealing. The characteristic peaks of TiO_2 (anatase) and Au are highlighted. (c) The TiO_2 average crystalline domain sizes for different deposition pressures and Au content calculated with Scherrer's equation.*

3.3 Optical properties

Figs. 4 and 5 show the transmittance spectra in the UV-vis-NIR range (300-2000 nm) of films deposited at 5 and 8 Pa before and after the thermal treatment, respectively, for which the Au content is listed in Table 1. The decrease of transmittance in the UV range is related with TiO_2 absorption [8]; conversely, in the visible-IR range there is a high-transparency region showing fringes as a consequence of interference phenomena, which depend on sample morphology, thickness and optical properties [57].

Before annealing (Fig. 4), Au in the TiO_2 film produces a transmittance decrease in the visible range at both deposition pressures. Specifically, 8 Pa Au-TiO_2 films (Fig. 4b) show a clear LSPR peak around 540 nm for the highest Au contents, for which Au NPs are observed in the as-deposited films (Fig. 1d). At low Au content, Au cluster size and density are too small to produce LSPR and a clear plasmonic effect. On the other hand, 5 Pa Au-TiO_2 films (Fig 4a) do not show a characteristic plasmonic absorption, which also can be related to the presence of Au layers with very small clusters and limited crystallinity, as discussed above (Fig. 1c). Notably, for the highest Au content (5% at.) the transmittance decreases strongly and this phenomenon is associated with the large amount of Au which absorb significantly in the analysed range, as we have shown in our previous paper [40].

The optical reflectance of Au-TiO_2 films is almost constant (around 20% and 10% for films deposited at 5 and 8 Pa, respectively) for all the wavelengths, therefore the observed decrease in transmittance can be associated to optical absorption of the system (see SI2).

The general effect of the thermal treatment is to slightly decrease the film transmittance, as already observed in TiO_2 films deposited without Au [45,51]. 5 Pa Au-TiO_2 annealed films (Fig. 5a) exhibit a plasmonic peak around 575 nm, while annealing on 8 Pa films (Fig. 5b) induces a more intense and well-defined plasmonic peak with respect to the corresponding as-deposited films (Fig. 4b), red-shifted to 560-570 nm. These effects can be related to the plasmonic behaviour of Au NPs which aggregate and grow upon thermal treatment. Moreover, the crystallization of TiO_2 leading to an increase of refractive index of the matrix (from 2.0-2.2 for amorphous TiO_2 up to 2.5 for anatase [58]) surrounding Au NPs may contribute to the redshift [59]. Notably, the LSPR position (i.e.

the transmission minimum) of annealed Au-TiO_2 films is similar at both deposition pressures as a consequence of comparable Au NP size, while the Au content mainly affects the absorption intensity.

Fig. 5c shows that the average transmittance of annealed samples in the visible range (390-750 nm) decreases with Au content at both deposition pressures. For 8 Pa Au-TiO_2 films, transmittance decreases from 96, for pure TiO_2, to 17% for films with 2.9% at. Au, while for 5 Pa films it drops from 85% to almost 0% with 3.5% at. Au.

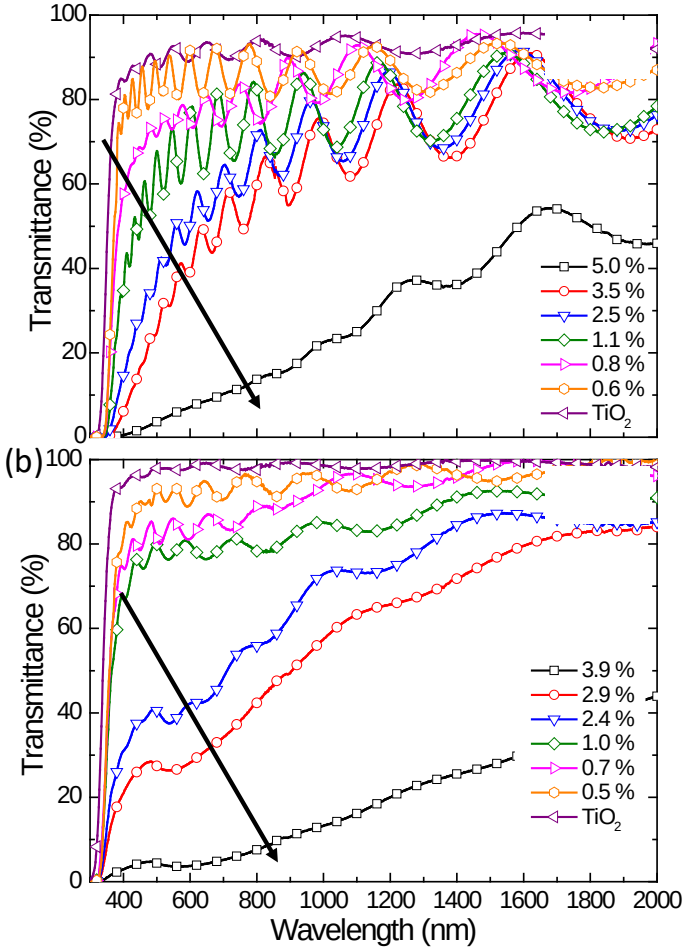

Figure 4*. Optical transmittance of Au-TiO_2 films deposited at (a) 5 Pa and (b) 8 Pa with different Au contents before thermal treatment.*

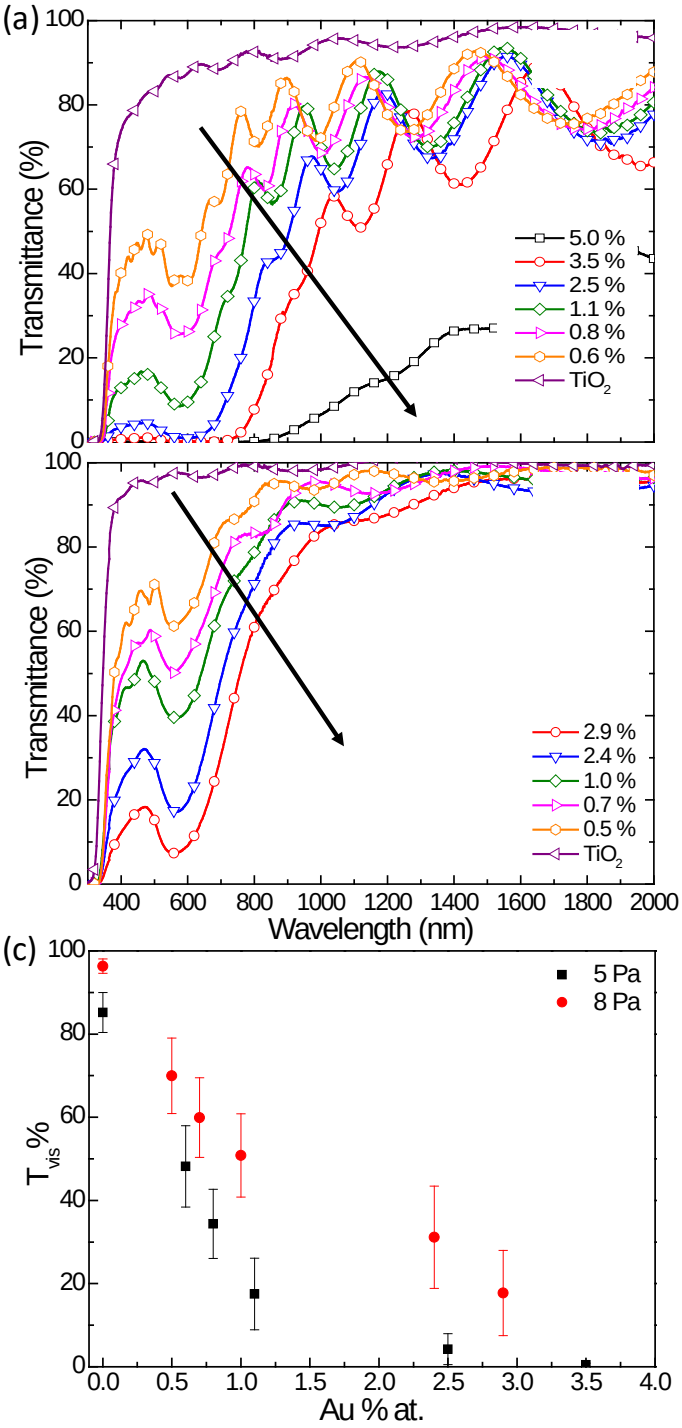

***Figure 5**. Optical transmittance of annealed Au-TiO_2 films deposited at (a) 5 Pa and (b) 8 Pa with different Au contents. (c) Average transmittance of annealed samples in the visible range (390-750nm) as a function of Au content at both deposition pressures.*

3.4 Photodegradation activity

As TiO_2 nanostructures are widely exploited for assisting the photodegradation of environmental pollutants, the photocatalytic properties of both TiO_2 and Au-TiO_2 nanostructured thin films were challenged in photodegradation tests of organic dyes. Methyl orange (MO) was selected as a typical degradation target, because of its mutagenic nature and high persistency [60]. For this test, annealed films deposited at 8 Pa were employed because of their high porosity, which makes them suitable in view of photocatalytic applications. In the case of integrated Au-TiO_2 thin films, samples with a gold content of 0.7 and 2.9 % at. were chosen in order to have a defined plasmonic peak. The experiments were carried out with a solar simulator (see Experimental details), in order to study the behaviour of the samples under natural sunlight and the photocatalytic activity was evaluated by monitoring the decrease in intensity of the MO main absorbance band in the visible (λ=460 nm) [61].

Fig. 6 shows the progress of MO photodegradation, expressed in terms of the A/A_0 ratio, where A_0 is the absorbance of the initial MO solution (concentration: 10^{-5} M, pH=4.2) and A is the absorbance at a given irradiation time. The MO self-degradation in the absence of any catalytic support was also considered as a reference. Before starting irradiation, the three samples were kept under dark for 60 minutes to take the adsorption effect into account. It is important to note that all the MO samples were simultaneously irradiated under the same conditions, in order to ensure a reliable comparison among absorbance data from different samples. Moreover, the temperature of the MO solution during irradiation was around 33°C, which excludes thermal effects as a primary cause of degradation. We note that, in spite of the mild irradiation conditions, the nanostructured TiO_2 films exhibit good photocatalytic efficiency, allowing to reduce the concentration of the MO solution to about 60% of its initial value in the first 60 minutes of irradiation and to about 20% in 240 minutes.

These data are particularly relevant, also in comparison to literature [62-64], due to the very small amount of TiO_2 that is loaded on the thin film support, in the order of 10^{-1}mg. Moreover, we compared

results of tree-like TiO_2 film with a reference planar TiO_2 thin film with the same geometric area synthetized with atomic layer deposition. The photocatalytic activity of PLD forest-like samples turned out to be significantly higher than that of planar thin films, as expected (see SI3). As the fraction of UV light in the solar lamp output is around 4% of the total irradiation, this remarkable activity might be ascribed to different effects, such as the presence of surface defects (oxygen vacancies, Ti^{3+} sites) and/or dye-sensitization, as already reported in literature [65-67]. Indeed, we have already demonstrated that hierarchical tree-like TiO2 structures favor photoconversion also by combining nano/mesoscale porosity beneficial for the penetration of the organic molecules through the film, a very large surface area and strong light scattering effects [41,43,45].

The integration of 0.7% at. Au in the TiO_2 nanostructures results in a small, yet significant improvement of the photocatalytic activity of the films, reducing the concentration of MO to less than 50% of its initial value after 60 minutes and to about 10% in 240 minutes. Although the study of the catalytic mechanisms is beyond the scope of this work, these data suggest that the presence of Au NPs can improve the catalytic activity of bare TiO_2 or favour the production of superoxide radicals, as recently discussed by Tsuji et al. [68]. It is known in fact that the presence of Au NPs is expected to make the e^-/h^+ separation more efficient, thus reducing recombinations, as reported in literature for analogous system [69,70]. On the other hand, due to the excitation of the LSPR in Au NP, plasmonic-related effects such as increased light scattering or hot electron generation can contribute to the enhanced photocatalytic activity [5]. We tested also Au-TiO_2 films with 2.9% at. Au and we observed a decrease of the photocatalytic activity with respect to the one with 0.7% at. Au, which may related to light absorption by Au and/or reduction of the active TiO_2 surface [7,71]. Further tests with other organic pollutants are in progress to elucidate the photocatalytic mechanisms and find optimal conditions, such as Au content, for developing thin-film photocatalytic supports with superior efficiency.

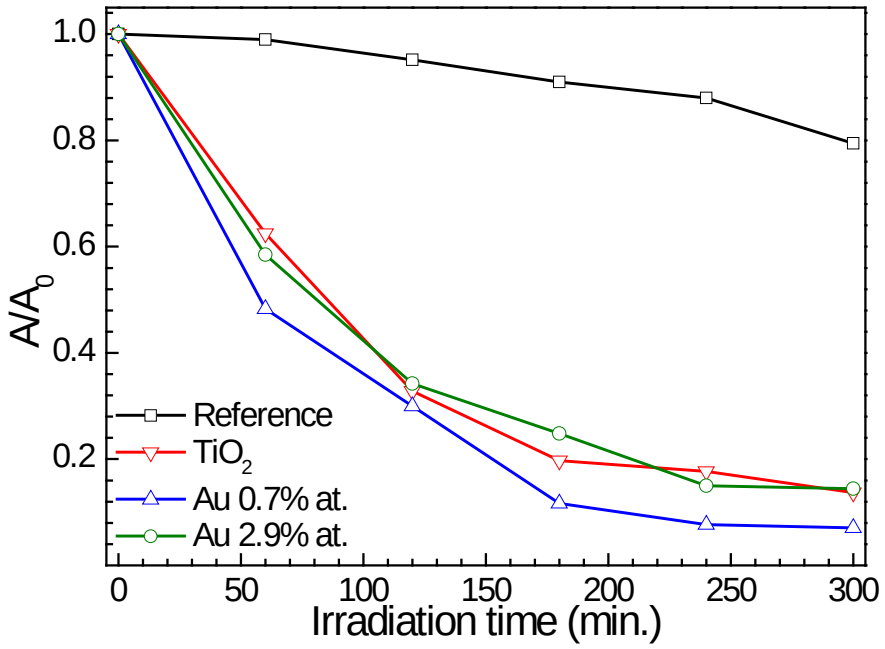

Figure 6. *A/A_0 as a function of time for pure TiO_2 and Au-TiO_2 films with 0.7 and 2.9 % at. Au deposited at 8 Pa. The error bars are included within the point size.*

4. Conclusions

In this work the integration of plasmonic Au NPs in hierarchical TiO_2 nanostructures has been reached with a single step synthesis through a vapor phase pulsed laser co-deposition approach. The effect of the Au content (0.5-5% at.) has been studied at two different TiO_2 porosities by depositing at different background pressures, 5 and 8 Pa of O_2. From SEM and TEM analyses it was observed that the integration of Au leads to a more compact film morphology; moreover, the deposition pressure affects the morphological organization of Au, i.e. 5 Pa films show a layered structure in which TiO_2 is separated by 10 nm-thick Au-rich layers, while 8 Pa films show Au in form of NPs homogeneously distributed in the porous TiO_2. These results highlight how the deposition pressure influences the clustering of Au and how it is possible to obtain NPs homogeneously dispersed in a semiconducting matrix without any thermal treatment, which is difficult to obtain with other physical vapor deposition techniques.

Then, the effect of the thermal treatment on the materials structure/morphology was studied. Annealing at 500 °C in air induces TiO_2 crystallization in anatase phase, while providing energy for Au diffusion leading to Au NPs formation and growth by coalescence and Ostwald ripening mechanisms.

XRD shows that the average anatase crystalline domain size (in the range 20-50 nm) slightly decreases both when increasing the deposition pressure and upon Au integration. Very small crystalline Au NPs are present in as deposited films, while thermal treatment induces the growth of larger Au crystalline domains as revealed by XRD. TEM analysis permits to investigate in detail the smallest Au NPs present in the integrated layers, showing an increase of NPs density and average size (from 3 to 5 nm) vs. Au content for annealed 5 Pa films, while TEM images of annealed 8 Pa films show an almost constant Au NPs diameter (around 3 nm) upon increasing Au content from 0.7 to 2.9% at.

Optical analysis indicates that for as deposited 5 Pa films absorption in the visible range (370-750 nm) increases with Au content, but a well-defined plasmonic resonance is not observed, while, after annealing, absorption further increases and a plasmonic peak clearly appears around 575 nm. For 8 Pa films, a plasmonic peak at about 540 nm is visible before annealing (for high Au amount), while annealing induces an increase in the plasmonic absorption (for all Au contents) and a red-shift of about 20 nm with respect to as deposited films.

Finally, we tested the photocatalytic properties of both TiO_2 and Au-TiO_2 (Au 0.8% at.) annealed films deposited at 8 Pa for the photodegradation of methyl orange under simulated natural sunlight. Pure nanoporous TiO_2 show relevant results with respect to literature, and the addition of Au NPs results in a further increase of the photocatalytic activity.

Overall, our results demonstrate the feasibility of one-step synthesis of Au NPs-TiO_2 integrated nanostructures via PLD and suggest the potentiality of this approach to be extended to other NP/oxide systems with controlled plasmonic response. Moreover, besides photocatalysis, these systems can be exploited for other plasmonic applications, especially those requiring nanoscale porosity and light scattering, such as chemical sensors, spectroscopy (e.g. SERS) and light management. Indeed, thanks to the versatility of the laser ablation process, it is in principle possible to tune the properties of the deposited species, among which morphology and structure, which allows the control of optical behavior of materials, e.g. the LSPR of embodied NPs, paving the way toward novel plasmonic-based devices.

Data availability

The raw/processed data required to reproduce these findings cannot be shared at this time due to technical or time limitations.

References

[1] Atwater, H. A.; Polman, A. Plasmonics for Improved Photovoltaic Devices. *Nat. Mater.* **2010,** *9***,** 205–213.

[2] Schuller, J. A.; Barnard, E. S.; Cai, W.; Chul Jun, Y.; White, J. S.; Brongersma, M. I. Plasmonics for Extreme Light Concentration and Manipulation. *Nat. Mater.* **2010**, *9***,** 193–204.

[3] Warren, S. C.; Thimsen, E. Plasmonic Solar Water Splitting. *Energy Environ. Sci.* **2012**, *5,* 5133–5146.

[4] Fu, C.; Li, M.; Li, H.; Li, C.; Wu, X. G.; Yang, B. Fabrication of Au Nanoparticle/TiO2 Hybrid Films for Photoelectrocatalytic Degradation of Methyl Orange. *J. Alloys Compd.* **2017**, *692,* 727–733.

[5] Naldoni, A.; Riboni, F.; Guler, U.; Boltasseva A.; Shalaev V. M.; Kildishev, A. V., A. Solar-Powered Plasmon-Enhanced Heterogeneous Catalysis. *Nanophotonics* **2016**, *5,* 112–133.

[6] Fujishima, A.; Rao, T. N.; Tryk, D. A. Titanium Dioxide Photocatalysis. *J. Photochem. Photobiol. C Photochem. Rev.* **2000**, *1,* 1–21.

[7] Primo, A.; Corma, A.; García, H. Titania Supported Gold Nanoparticles as Photocatalyst. *Phys. Chem. Chem. Phys.* **2011**, *13,* 886–910.

[8] Tang, H.; Prasad, K.; Sanjinès, R.; Schmid, P. E.; Lévy, F. Electrical and Optical Properties of TiO2 Anatase Thin Films. *J. Appl. Phys.* **1994**, *7,* 2042–2047.

[9] Amendola, V.; Pilot, R.; Frasconi, M.; Maragò, O. M.; Iatì, M. A. Surface plasmon resonance in gold nanoparticles: a review. *Journal of Physics: Condensed Matter* **2017**, *29.20*, 203002.

[10] Pérez-Juste, J.; Pastoriza-Santos, I.; Liz-Marzán, L. M.; Mulvaney, P. Gold Nanorods: Synthesis, Characterization and Applications. *Coord. Chem. Rev.* **2005,** *249***,** 1870–1901.

[11] Kelly, K. L.; Coronado, E.; Zhao, L. L.; Schatz, G. C. The Optical Properties of Metal Nanoparticles: The Influence of Size, Shape, and Dielectric Environment. *J. Phys. Chem. B* **2003**, *107,* 668–677.

[12] Linic, S.; Christopher, P.; Ingram, D. B. Plasmonic-Metal Nanostructures for Efficient Conversion of Solar to Chemical Energy. *Nat. Mater.* **2011**, *10,* 911–921.

[13] Jain, P. K.; Huang, X.; El-Sayed, I. H.; El-Sayed, M. A. Noble Metals on the Nanoscale: Optical and Photothermal Properties and Some Applications in Imaging, Sensing, Biology, and Medicine. *Acc. Chem. Res.* **2008**, *41,* 1578–1586.

[14] Yue, G.; Su, S.; Li, N.; Shuai, M.; Lai, X.; Astruc, D.; Zhao, P. Gold nanoparticles as sensors in the colorimetric and fluorescence detection of chemical warfare agents. *Coordination Chemistry Reviews* **2016**, *311,* 75-84.

[15] Agarwal, N. R.; Neri, F.; Trusso, S.; Lucotti, A.; Ossi, P. M. Au Nanoparticle Arrays Produced by Pulsed Laser Deposition for Surface Enhanced Raman Spectroscopy. *Appl. Surf. Sci.* **2012**, *258,* 9148–9152.

[16] Krajczewski, J.; Kołątaj, K.; Kudelski, A. Plasmonic nanoparticles in chemical analysis. *RSC Advances* **2017**, *7.28*, 17559-17576.

[17] Fan, R.; Wang, L.; Chen, Y.; Zheng, G.; Li, L.; Li, Z.; Zhou, H. Tailored Au@ TiO 2 nanostructures for the plasmonic effect in planar perovskite solar cells. *Journal of Materials Chemistry A* **2017**, *5.24*, 12034-12042.

[18] Kreibig, U.; Vollmer, M. *Optical Properties of Metal Clusters*; Springer Science & Business Media, 2013.

[19] Gomes Silva, C.; Juárez, R.; Marino, T.; Molinari, R.; García, H. Influence of Excitation Wavelength (UV or Visible Light) on the Photocatalytic Activity of Titania Containing Gold Nanoparticles for the Generation of Hydrogen or Oxygen from Water. *J. Am. Chem. Soc.* **2011**, *133,* 595–602.

[20] Su, F.; Wang, T.; Lv, R.; Zhang, J.; Zhang, P.; Lu, J.; Gong, J., F. Dendritic Au/TiO2 Nanorod Arrays for Visible-Light Driven Photoelectrochemical Water Splitting. *Nanoscale* **2013**, *5,* 9001–9009.

[21] Mubeen, S.; Hernandez-Sosa, G.; Moses, D.; Lee, J.; Moskovits, M. Plasmonic Photosensitization of a Wide Band Gap Semiconductor: Converting Plasmons to Charge Carriers. *Nano Lett.* **2011**, *11,* 5548–5552.

[22] Wang, T.; Lv, R.; Zhang, P.; Li, C.; Gong, J. Au Nanoparticle Sensitized ZnO Nanopencil Arrays for Photoelectrochemical Water Splitting. *Nanoscale* **2015**, *7,* 77–81.

[23] Jang, J. S.; Yoon, K. Y.; Xiao, X.; Fan, F.R. F.; Bard, A. J. Development of a Potential Fe2O3-Based Photocatalyst Thin Film for Water Oxidation by Scanning Electrochemical Microscopy: Effects of Ag−Fe2O3 Nanocomposite and Sn Doping. *Chem. Mater.* **2009**, *21,* 4803–4810.

[24] Carraro, G.; Maccato, C.; Gasparotto, A.; Warwick, M. E.; Sada, C.; Turner, S.; Bazzo, A.; Andreau, T.; Pliekhova, O.; Korte, D.; Štangar, U. L.; Van Tendeloo, G.; Morante, J. R.; Barreca, D.; Hematite-based nanocomposites for light-activated applications: Synergistic role of TiO2 and Au introduction. *Solar Energy Materials and Solar Cells* **2017**, *159*, 456-466.

[25] Haruta, M. Size- and Support-Dependency in the Catalysis of Gold. *Catal. Today* **1997**, *36,* 153–166.

[26] Valverde-Aguilar, G.; García-Macedo, J. A.; Rentería-Tapia, V.; Aguilar-Franco, M. Photoconductivity Studies on Amorphous and Crystalline TiO2 Films Doped with Gold Nanoparticles. *Appl. Phys. A* **2011**, *103,* 659–663.

[27] Tian, Y.; Tatsuma, T. Mechanisms and Applications of Plasmon-Induced Charge Separation at TiO2 Films Loaded with Gold Nanoparticles. *J. Am. Chem. Soc.* **2005**, *127,* 7632–7637.

[28] Tamm, A.; Acik, I. O.; Arroval, T.; Kasikov, A.; Seemen, H.; Marandi, M.; Krunks, M.; Mere, A; Kukli, K.; Aarik, J. Plasmon Resonance Effect Caused by Gold Nanoparticles Formed on Titanium Oxide Films. *Thin Solid Films* **2016**, 616, 449–455.

[29] Cushing, B. L.; Kolesnichenko, V. L.; O'Connor, C. J. Recent Advances in the Liquid-Phase Syntheses of Inorganic Nanoparticles. *Chem. Rev.* **2004**, *104,* 3893–3946.

[30] Kharisov, B. I.; Kharissova, O. V.; García, B. O.; Méndez, Y. P.; Fuente, I. G. State of the Art of Nanoforest Structures and their Applications. *RSC Adv.* **2015**, *5,* 105507–105523.

[31] Qi, J.; Dang, X.; Hammond, P. T.; Belcher, A. M. Highly Efficient Plasmon-Enhanced Dye-Sensitized Solar Cells through Metal@Oxide Core–Shell Nanostructure. *ACS Nano* **2011**, *5,* 7108–7116.

[32] Rodrigues, M. S.; Costa, D.; Domingues, R. P.; Apreutesei, M.; Pedrosa, P.; Martin, N.; Correlo, V. M.; Reis, R. L.; Alves, E.; Barradas, N. P.; Sampaio, P.; Borges, J.; Vaz, F., M. S. Optimization of Nanocomposite Au/TiO2 Thin Films towards LSPR Optical-Sensing. *Appl. Surf. Sci.* **2017**, *438,* 74-83.

[33] Borges, J.; Pereira, R. M. S.; Rodrigues, M. S.; Kubart, T.; Kumar, S.; Leifer, K.; Cavaleiro, A.; Polcar, T.; Vasilevskiy, M. I.; Vaz, F. Broadband Optical Absorption Caused by the Plasmonic Response of Coalesced Au Nanoparticles Embedded in a TiO2 Matrix. *J. Phys. Chem. C* **2016**, *120,* 16931–16945.

[34] Borges, J.; Kubart, T.; Kumar, S.; Leifer, K.; Rodrigues, M. S.; Duarte, N.; Martins, B.; Dias, J. P.; Cavaleiro, A.; Vaz, F., J. Microstructural Evolution of Au/TiO2 Nanocomposite Films: The influence of Au Concentration and Thermal Annealing. *Thin Solid Films* **2015**, *580,* 77–88.

[35] Eason, R. *Pulsed Laser Deposition of Thin Films: Applications-Led Growth of Functional Materials*; John Wiley & Sons, 2007.

[36] Srivastava, A. K. *Oxide Nanostructures: Growth, Microstructures, and Properties*; CRC Press, 2014.

[37] Donnelly, T.; Krishnamurthy, S.; Carney, K.; McEvoy, N.; Lunney, J. G. Pulsed Laser Deposition of Nanoparticle Films of Au. *Appl. Surf. Sci.* **2007**, *254***,** 1303–1306.

[38] Domingo, C.; Resta, V.; Sanchez-Cortes, S.; Garcia-Ramos, J. V.; Gonzalo, J. Pulsed Laser Deposited Au Nanoparticles as Substrates for Surface-Enhanced Vibrational Spectroscopy. *J. Phys. Chem. C* **2007**, *111,* 8149–8152.

[39] Gonzalo, J.; Perea, A.; Babonneau, D.; Afonso, C. N.; Beer, N.; Barnes, J. P.; Petford-Long, A. K.; Hole, D. E.; Townsend, P. D. Competing Processes During the Production of Metal Nanoparticles by Pulsed Laser Deposition. *Phys. Rev. B* **2005**, *71***,** 125420.

[40] Ghidelli, M.; Mascaretti, L.; Bricchi, B. R.; Zapelli, A.; Russo, V.; Casari, C. S.; Li Bassi, A. Engineering Plasmonic Nanostructured surfaces by Pulsed Laser Deposition. *Appl. Surf. Sci.* **2018**, *434,* 1064–1073.

[41] Di Fonzo, F.; Casari, C. S.; Russo, V.; Brunella, M. F.; Li Bassi, A.; Bottani, C. E. Hierarchically Organized Nanostructured TiO2 For Photocatalysis Applications. *Nanotechnology* **2009**, *20,* 15604.

[42] Fusi, M.; Maccallini, E.; Caruso, T.; Casari, C. S.; Li Bassi, A.; Bottani, C. E.; Rudolf, P.; Prince, K. C.; Agostino, R. G. Surface Electronic and Structural Properties of Nanostructured Titanium Oxide Grown by Pulsed Laser Deposition. *Surf. Sci.* **2011**, *605,* 333–340.

[43] Sauvage, F.; Di Fonzo, F.; Li Bassi, A.; Casari, C. S.; Russo, V.; Divitini, G.; Ducati, C.; Bottani, C. E.; Comte, P.; Graetzel, M. Hierarchical TiO2 Photoanode for Dye-Sensitized Solar Cells. *Nano Lett.* **2010**, *10,* 2562–2567.

[44] Noh, J. H.; Park, J. H.; Han, H. S.; Kim, D. H.; Han, B. S.; Lee, S.; Kim, J. Y.; Jung, H. S.; Hong, K. S. Aligned Photoelectrodes with Large Surface Area Prepared by Pulsed Laser Deposition. *J. Phys. Chem. C* **2012**, *116,* 8102–8110.

[45] Passoni, L.; Ghods, F.; Docampo, P.; Abrusci, A.; Martí-Rujas, J.; Ghidelli, M.; Divitini, G.; Binda, M.; Guarnera, S.; Li Bassi, A.; Casari, C. S.; Snaith, H. J.; Petrozza, A.; Di Fonzo, F. Hyperbranched Quasi-1D Nanostructures for Solid-State Dye-Sensitized Solar Cells. *ACS Nano* **2013**, *7,* 10023–10031.

[46] Divitini, G.; Stenzel, O.; Ghadirzadeh, A.; Guarnera, S.; Russo, V.; Casari, C. S.; Li Bassi, A.; Petrozza, A.; Di Fonzo, F.; Schmidt, V.; Ducati, C. Nanoscale Analysis of a Hierarchical Hybrid Solar Cell in 3D. *Adv. Funct. Mater.* **2014**, *24,* 3043–3050.

[47] Matarrese, R.; Nova, I.; Li Bassi, A. L.; Casari, C. S.; Russo, V. Hierarchical Nanostructured TiO2 Films Prepared by Reactive Pulsed Laser Position for Photoelectrochemical Water Splitting. *Chem. Eng. Trans.* **2014**, *41,* 313–318.

[48] Hanaor, D. A.; Sorrell, C. C. Review of the Anatase to Rutile Phase Transformation. *J. Mater. Sci.* **2011**, *46,* 855–874.

[49] Pawley, G. S. Unit-Cell Refinement from Powder Diffraction Scans. *J. Appl. Crystallogr.* **1981**, *14,* 357–361.

[50] Matarrese, R.; Nova, I.; Li Bassi, A.; Casari, C. S.; Russo, V.; Palmas, S. Preparation and Optimization of TiO2 Photoanodes Fabricated by Pulsed Laser Deposition for Photoelectrochemical Water Splitting. *J. Solid State Electrochem.* **2017**, *21,* 3139-3154.

[51] Mascaretti, L.; Ferrulli, S.; Mazzolini, P.; Casari, C. S.; Russo, V.; Matarrese, R.; Nova, I.; Terraneo, G.; Liu, N.; Schmuki, P. Hydrogen-Treated Hierarchical Titanium Oxide Nanostructures for Photoelectrochemical Water Splitting. *Sol. Energy Mater. Sol. Cells* **2017**, *169,* 19–27.

[52] Borges, J.; Rodrigues, M. S.; Kubart, T.; Kumar, S.; Leifer, K.; Evaristo, M.; Cavaleiro, A.; Apreutesei, M.; Pereira, R. M. S.; Vasilevskiy, M. I.; Polcar, T.; Vaz, F. Thin Films Composed of Gold Nanoparticles Dispersed in a Dielectric Matrix: The Influence of the Host Matrix on the Optical and Mechanical Responses. *Thin Solid Films* **2015**, *596,* 8–17.

[53] Parker, S. C.; Campbell, C. T. Kinetic Model for Sintering of Supported Metal Particles with Improved Size-Dependent Energetics and Applications to Au on TiO2. *Phys. Rev. B* **2007**, *75,* 35430.

[54] Moldovan, S.; Roiban, L.; Georgescu, D.; Baia, L.; Ersen, O. Thermal Evolution of Silver Nanoparticles onto Porous TiO2 Nanostructures. *Catal. Today* **2017**, *284,* 221–228.

[55] Chichagov, A. V. Information-Calculating System on Crystal Structure Data of Minerals (MINCRYST). *Mater. Sci. Forum* **1994**, *166–169,* 193–198.

[56] Moore, D. M.; Reynolds, R. C. *X-ray Diffraction and the Identification and Analysis of Clay Minerals*. *332,* Oxford university press New York, 1989.

[57] Manifacier, J. C.; Gasiot, J.; Fillard, J. P. A Simple Method for the Determination of the Optical Constants n, k and the Thickness of a Weakly Absorbing Thin Film. *J. Phys. E* **1976**, *9,* 1002.

[58] Torrell, M.; Kabir, R.; Cunha, L.; Vasilevskiy, M. I.; Vaz, F.; Cavaleiro, A.; Alves, E.; Barradas, N. P. Tuning of the Surface Plasmon Resonance in TiO2/Au Thin Films Grown by Magnetron Sputtering: The Effect of Thermal Annealing. *J. Appl. Phys.* **2011**, *109,* 74310.

[59] Torrell, M.; Cunha, L.; Kabir, M. R.; Cavaleiro, A.; Vasilevskiy, M. I.; Vaz, F. Nanoscale Color Control of TiO2 Films with Embedded Au Nanoparticles. *Mater. Lett.* **2010**, *64,* 2624–2626.

[60] Al-Qaradawi, S.; Salman, S. R. Photocatalytic Degradation of Methyl Orange as a Model Compound. *Semicond. Photochem. 1 FIRST Int. Conf. Semicond. Photochem. Strathclyde Glasg. JULY 2001* **2002**, *148,* 161–168.

[61] Gjipalaj, J.; Alessandri, I. Easy Recovery, Mechanical Stability, Enhanced Adsorption Capacity and Recyclability of Alginate-Based TiO2 Macrobead Photocatalysts for Water Treatment. *J. Environ. Chem. Eng.* **2017**, *5,* 1763–1770.

[62] Parida, K. M.; Sahu, N.; Biswal, N. R.; Naik, B.; Pradhan, A. C. Preparation, Characterization, and Photocatalytic Activity of Sulfate-Modified Titania for Degradation of Methyl Orange under Visible Light. *J. Colloid Interface Sci.* **2008**, *318,* 231–237.

[63] Ho, L. N.; Ong, S. A.; Osman, H.; Chong, F. M. Enhanced Photocatalytic Activity of Fish Scale Loaded TiO2 Composites Under Solar Light Irradiation. *J. Environ. Sci.* **2012**, *24,* 1142–1148.

[64] Azad, K.; Gajanan, P. Photodegradation of Methyl Orange in Aqueous Solution by the Visible Light Active Co: La: TiO2 Nanocomposite. *Chem Sci J* **2017**, *8,* 164.

[65] Pan, X.; Yang, M. Q.; Fu, X.; Zhang, N.; Xu, Y. J. Defective TiO2 with Oxygen Vacancies: Synthesis, Properties and Photocatalytic Applications. *Nanoscale* **2013**, *5,* 3601–3614.

[66] Yan, Z.; Gong, W.; Chen, Y.; Duan, D.; Li, J.; Wang, W.; Wang, J. Visible-Light Degradation of Dyes and Phenols over Mesoporous Titania Prepared by Using Anthocyanin from Red Radish as Template. *International Journal of Photoenergy* **2014**.

[67] Vinu, R.; Polisetti, S.; Madras, G. Dye Sensitized Visible Light Degradation of Phenolic Compounds. *Chem. Eng. J.* **2010**, *165,* 784–797.

[68] Tsuji, M.; Matsuda, K.; Tanaka, M.; Kuboyama, S.; Uto, K.; Wada, N.; Kawazumi, H.; Tsuji, T.; Ago, H.; Hayashi, J. I. Enhanced Photocatalytic Degradation of Methyl Orange by Au/TiO2 Nanoparticles under Neutral and Acidic Solutions. *ChemistrySelect* **2018,** *3*, 1432–1438.

[69] Chiarello, G. L.; Selli, E.; Forni, L. Photocatalytic hydrogen production over flame spray pyrolysis-synthesised TiO2 and Au/TiO2. *Appl. Catal. B Environ.* **2008,** *84*, 332–339.

[70] Ayati, A.; Ahmadpour, A.; Bamoharram, F. F.; Tanhaei, B.; Mänttäri, M.; Sillanpää, M. A Review on Catalytic Applications of Au/TiO2 Nanoparticles in the Removal of Water Pollutant. *Chemosphere* **2014**, *107,* 163–174.

[71] Oros-Ruiz, S.; Gómez, R.; López, R.; Hernandez-Gordillo, A.; Pedraza-Avella, J. A.; Moctezuma, E.; Pérez, E. Photocatalytic reduction of methyl orange on Au/TiO2 semiconductors. *Catal. Commun.* **2012,** *21*, 72–76.